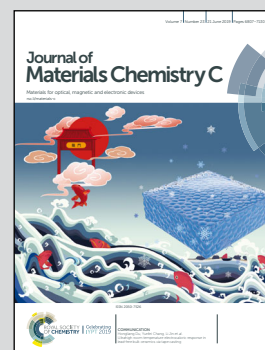


Showcasing research from the School of Physics and Optoelectronic Engineering, Xidian University and the National Center for Nanoscience and Technology, China.

Few-layer $\text{ReS}_{2(1-x)}\text{Se}_{2x}$ nanoflakes for noise-like pulse generation in a mode-locked ytterbium-doped fiber laser

By using few-layer ternary $\text{ReS}_{1.02}\text{Se}_{0.98}$ nanoflakes, one can realize passive Q-switch and noise-like pulses operating in an ytterbium-doped fiber laser. The results demonstrate that $\text{ReS}_{1.02}\text{Se}_{0.98}$ has potential applications in optical modulators, and opens up new application opportunities for these novel materials in nonlinear optics and ultrafast photonic technologies.

As featured in:



See Junli Wang et al.,
J. Mater. Chem. C, 2019, 7, 6900.



ROYAL SOCIETY
OF CHEMISTRY

Celebrating
IYPT 2019

rsc.li/materials-c

Registered charity number: 207890

Cite this: *J. Mater. Chem. C*, 2019,
7, 6900

Few-layer $\text{ReS}_{2(1-x)}\text{Se}_{2x}$ nanoflakes for noise-like pulse generation in a mode-locked ytterbium-doped fiber laser

Mengyuan Ma,^{†a} Wen Wen,^{†bc} Yao Zhang,^{id a} Chenxi Dou,^{id a}
Junli Wang,^{id *ad} Liming Xie,^{id bc} Ching-Hwa Ho^{id e} and Zhiyi Wei^{id f}

We investigated the ternary $\text{ReS}_{2(1-x)}\text{Se}_{2x}$ alloys and fabricated few-layer $\text{ReS}_{1.02}\text{Se}_{0.98}$ nanoflakes to realize passive Q-switch and noise-like pulses operating at 1 μm wavelength. Stable Q-switching pulses can be achieved with a threshold pump power of 180 mW and a maximum pump power of 300 mW. The single pulse energy of 81.47 nJ and pulse width as narrow as 2.2 μs at 1035 nm center wavelength were achieved. By optimizing the parameters of the cavity, self-started noise-like pulses were realized, which are centered at 1031 nm. The average pulse width of the spike was 283 fs on the top of a broad pedestal and the fundamental repetition was 38.98 MHz. Our work demonstrates that $\text{ReS}_{1.02}\text{Se}_{0.98}$ has potential applications in optical modulators, and also opens up new application opportunities for these novel materials in nonlinear optics and ultrafast laser photonic technologies.

Received 1st February 2019,
Accepted 13th May 2019

DOI: 10.1039/c9tc00625g

rsc.li/materials-c

Introduction

The generation and manipulation of optical pulses have attracted great attention in the fiber laser research community within the past few years owing to their significant potential in high-speed communications, material processing and medical diagnosis.^{1–3} In passively Q-switched and mode-locked techniques, using the real saturable absorber (SA) is a simple and the most effective method to obtain laser pulses.^{4–6} In this regard, various types of physical SAs have been extensively investigated, such as topological insulators (TIs),^{7,8} black phosphorus (BP)⁹ and carbon nanotubes (CNTs),¹⁰ which have already been applied in various Q-switched and mode-locked fiber laser designs.

Besides the traditional mode-locked picosecond and femtosecond pulses, passively mode-locked fiber lasers based on SA can also emit a so-called noise-like pulse (NLP), which was firstly demonstrated by Horowitz *et al.* in 1997.¹¹ Compared with other

regular pulses, the NLP is essentially a pulse wave packet composed of a bunch of random femtosecond or picosecond ultrashort pulses by a soliton collapse effect and cavity positive feedback.¹² Hence it possesses a distinguishable autocorrelation trace characterized by a narrow peak located on the substrate of picosecond or nanosecond order. The overall contour of the pulse resembles noise, so it is called an NLP.¹³ In general, the burst of NLPs is an inherent property for mode-locked cavities operating in strong pumping or high-gain conditions, and their formation is independent of the configuration or dispersion regime of the cavity.^{14,15} To date, most mode-locked lasers used to study NLP have been implemented using nonlinear polarization rotation (NPR) techniques.^{16–18} Although there are a few reports on NLP using graphene,¹⁹ topological insulators,^{20,21} black phosphorus²² and WS_2 ,^{15,23} using other novel SA materials has not been reported yet.

In recent years, low-dimensional nanomaterials transition metal dichalcogenides (TMDs), including molybdenum disulphide (MoS_2),²⁴ tungsten disulphide (WS_2),²⁵ and their analogue (tungsten diselenide, WSe_2),²⁶ have received significant attention because of their semiconducting property with tunable bandgaps and natural abundance.^{27,28} Compared with the many binary TMDs, ternary TMDs, like rhenium sulfide selenide ($\text{ReS}_{1.02}\text{Se}_{0.98}$), has received little attention in the study of SAs. Similar to the other TMD materials, the layers in the bulk crystals are stacked together by relatively weak van der Waals forces, making them relatively easy to exfoliate into single and few layer forms. The reported bandgap of $\text{ReS}_{1.02}\text{Se}_{0.98}$ can be continuously tuned from 1.62 to 1.31 eV due to size and chemical differences between two

^a School of physics and optoelectronics Engineering, Xidian University, Xi'an 710071, China. E-mail: dispersion@126.com

^b CAS Key Laboratory of Standardization and Measurement for Nanotechnology, CAS Center for Excellence in Nanoscience, National Center for Nanoscience and Technology, Beijing 100190, China

^c University of Chinese Academy of Sciences, Beijing 100049, People's Republic of China

^d State Key Laboratory of Pulsed Power Laser Technology, Hefei 230037, China

^e Graduate Institute of Applied Science and Technology, National Taiwan University of Science and Technology, Taipei 106, Taiwan, Republic of China

^f Beijing Nation Laboratory for Condensed Matter Physics, Institute of Physics, Chinese Academy of Sciences, Beijing 100190, China

[†] These authors contributed equally.

constituent elements,^{29,30} which suggests that the ternary TMD bandgap could be varied by changing not only the thickness but also the proportion of S and Se. The $\text{ReS}_{1.02}\text{Se}_{0.98}$ has a high damage threshold, which facilitates the generation of high-energy NLPs. Therefore, it is meaningful to investigate the ultrafast optical properties of ternary $\text{ReS}_{1.02}\text{Se}_{0.98}$ in passively Q-switched and mode-locked fiber lasers.

In this article, we demonstrate Q-switched operation and the generation of NLP in an ytterbium-doped fiber (YDF) laser using the $\text{ReS}_{1.02}\text{Se}_{0.98}$ absorber. The nonlinear absorption characteristics of $\text{ReS}_{1.02}\text{Se}_{0.98}$ are obtained by a twin detector technique. The results indicate a modulation depth of $\sim 2.9\%$ and saturating intensity of $\sim 0.13 \text{ MW cm}^{-2}$ at 1030 nm. The fiber laser can generate output pulses with a narrow pulse width of 2.2 μs and a corresponding pulse energy of 81.47 nJ. The fundamental noise-like mode-locked pulses possess an output spectral bandwidth of 3.9 nm and a repetition rate of 34.77 MHz. Because the NLP lasers do not require high modulation depth SAs, and the modulation depth of $\text{ReS}_{1.02}\text{Se}_{0.98}$ is relatively low, it is suitable for NLP generation. To the best of our knowledge, this is the first experimental demonstration of noise-like mode locking in a YDF laser based on $\text{ReS}_{1.02}\text{Se}_{0.98}$ -SA in an all normal dispersion regime.

Few-layer $\text{ReS}_{1.02}\text{Se}_{0.98}$ fabrication

Single crystals of the $\text{ReS}_{2(1-x)}\text{Se}_{2x}$ solid solution series were grown by the chemical vapor transport method using Br_2 as a transport agent.³¹ The 2D $\text{ReS}_{1.02}\text{Se}_{0.98}$ nanoflakes we used were fabricated by mechanical exfoliation. The lattice vibration dynamics were characterized by Raman spectroscopy. Because the $\text{ReS}_{1.02}\text{Se}_{0.98}$ belongs to the C_i point group, 18 active Raman modes are allowed. A series of Raman peaks ranging from 100 to 500 cm^{-1} demonstrate that the exfoliated nanoflakes are $\text{ReS}_{1.02}\text{Se}_{0.98}$ (Fig. 1a). The crystal structure of $\text{ReS}_{1.02}\text{Se}_{0.98}$ was further validated by high-resolution transmission electron microscopy (HR-TEM). Fig. 1b shows a set of lattice planes with an interplane distance of 0.34 nm, which can be attributed to

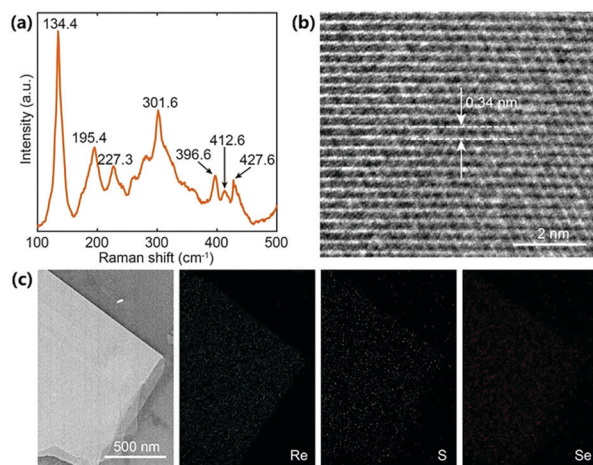


Fig. 1 (a) Raman spectrum and (b) HRTEM image of a $\text{ReS}_{1.02}\text{Se}_{0.98}$ flake. (c) SEM image, and EDS elemental mappings of Re, S and Se.

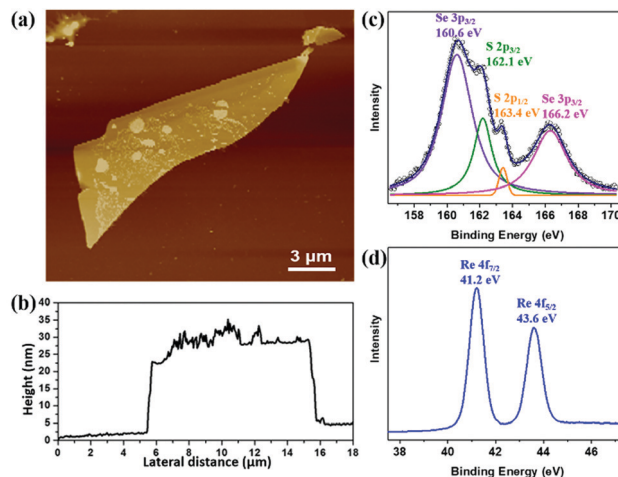


Fig. 2 (a) AFM image of the $\text{ReS}_{1.02}\text{Se}_{0.98}$ flake. (b) Height profiles of the nanosheet. XPS spectra: (c) S 2p, Se 3p; (d) Re 4f.

the distance of Re atomic chains. The composition of $\text{ReS}_{1.02}\text{Se}_{0.98}$ was characterized by energy dispersive spectroscopy (EDS) under scanning electron microscopy (SEM), as shown in Fig. 1c. The EDS elemental mappings present the homogeneous spatial distribution of Re, S and Se elements, indicating the successful fabrication of this ternary alloy.

The typical atomic force microscopy (AFM) image of the exfoliated $\text{ReS}_{1.02}\text{Se}_{0.98}$ dropped on Si/SiO₂ substrates reveals the profile of the slice, as depicted in Fig. 2a. Height-profiling of the nanosheet shown in Fig. 2b suggests that the average thickness of one nanosheet is 27 nm. The composition of the $\text{ReS}_{1.02}\text{Se}_{0.98}$ flakes is confirmed by X-ray photoelectron spectroscopy (XPS). The peaks at 162.1, 163.4, 160.6 and 166.2 eV are attributed to 2p_{3/2} and 2p_{1/2} orbitals of S²⁻ and 3p_{3/2} and 3p_{1/2} orbitals of Se²⁻, respectively, as shown in Fig. 2c. The bonding configurations of Re are shown in Fig. 2d, and two characteristic peaks located at 41.2 eV and 43.6 eV correspond to the 4f_{7/2} and 4f_{5/2} level peaks of Re⁴⁺, respectively. The ratio (*R*) of Re, S and Se atoms is measured to be 1 : 1.02 : 0.98.

The $\text{ReS}_{1.02}\text{Se}_{0.98}$ -based SA we used was prepared using the mechanical exfoliation technique with Scotch tape. This process is illustrated in Fig. 3(a)–(e). The $\text{ReS}_{1.02}\text{Se}_{0.98}$ flake is first placed on a piece of scotch tape, afterwards the scotch tape is refolded many times. Then by transferring $\text{ReS}_{1.02}\text{Se}_{0.98}$ flakes onto the

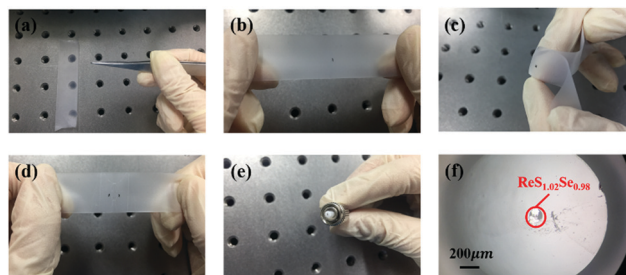


Fig. 3 $\text{ReS}_{1.02}\text{Se}_{0.98}$ mechanical exfoliation process and transfer onto the fiber ferrule.

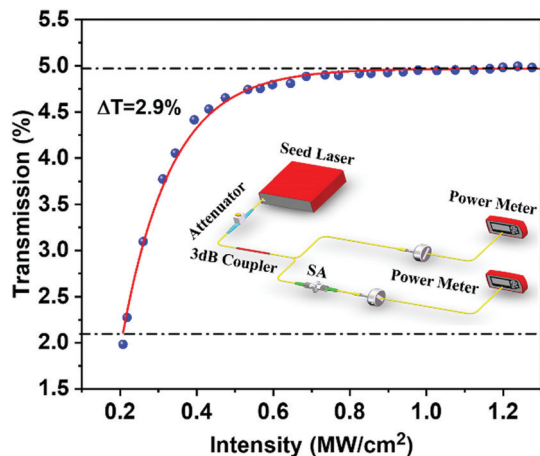


Fig. 4 The transmission of $\text{ReS}_{1.02}\text{Se}_{0.98}$ SA. Inset: Experimental setup of nonlinear optical characterization.

standard FC/APC fiber end face, and connecting with another clean one by a standard flange adapter, an all-fiber structure is constructed. Fig. 3(f) is the microscope image of the FC/APC fiber ferrule end face. It can be seen that the ferrule core was covered with $\text{ReS}_{1.02}\text{Se}_{0.98}$ flakes.

The nonlinear absorption properties of the $\text{ReS}_{1.02}\text{Se}_{0.98}$ SA were investigated by using the twin-detector technique, as shown in the inset of Fig. 4. The pump source was a home-made Yb-doped Nonlinear Polarization Evolution (NPE) mode-locking fiber laser with a repetition of 58.24 MHz, pulse duration of 4 ps, and center wavelength of 1030 nm. A variable optical attenuator (VOA) was used for power regulation. The measured results and fitted curve with the following formula are shown in Fig. 4.

$$T(I) = 1 - \Delta T \times \exp(-I/I_{\text{sat}}) - A_{\text{ns}}$$

where $T(I)$ is transmission, ΔT is modulation depth, I is input intensity of the laser, I_{sat} is saturation intensity, and A_{ns} is non-saturable absorbance. From Fig. 3b, the modulation depth of the $\text{ReS}_{1.02}\text{Se}_{0.98}$ is evaluated to be 2.9%. The saturating intensity is about 0.13 MW cm^{-2} .

Ultrafast photonics applications

Q-switched fiber laser

The experimental setup of the $\text{ReS}_{1.02}\text{Se}_{0.98}$ SA based ytterbium-doped fiber laser (YDFL) is shown in Fig. 5. A 976 nm laser diode (LD) with a maximum output power of 600 mW was used as the pump source. The pump energy was delivered into the cavity *via* a 980/1030 wave division multiplexer (WDM). A piece of 55 cm long Yb-doped fiber (Liekki Yb 1200-4/125) with a dispersion parameter of $\sim 23 \text{ fs}^2 \text{ km}^{-1}$ was employed as the laser gain medium. An isolator (ISO) and a polarization controller (PC) were used for unidirectional operation and adjusting the polarization state in the cavity, respectively. An 8 nm bandpass filter (BPF) was added into the cavity for wavelength choosing. A 10:90 fiber-fused optical coupler (OC) was used to output the laser. The total length of the cavity was about 5.0 m; thus, the net dispersion

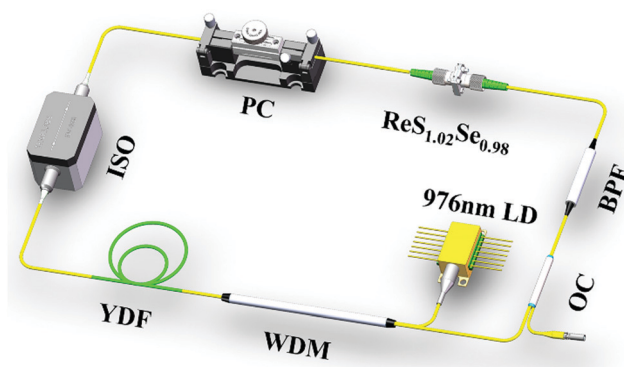


Fig. 5 Schematic of the Q-switched YDF laser cavity.

of the Yb-doped fiber laser was calculated to be 0.1 ps^2 . An optical spectrometer (Ocean Optics HR2000), a commercial autocorrelator (APE Pulse CheckUSB), and a real-time oscilloscope (Tektronix DPO3053, 500 MHz, 2.5GS/S) with a photodetector (Thorlabs DET10A/M) were employed to record the laser outputs.

In the fiber laser setup, Q-switched pulses were obtained at a pump power of $\sim 180 \text{ mW}$. When the pump power was 300 mW, the narrowest pulse width was obtained, as depicted in Fig. 6a. The measured corresponding optical spectrum, which centers at 1035 nm, is shown in Fig. 6b. In the observation over a one-hour period, the Q-switched spectrum exhibits considerably high stability. As illustrated in Fig. 6c, by adjusting the input pump power from 180 mW to 300 mW, the repetition rate linearly increases from 21.66 kHz to 36.33 kHz while the corresponding pulse duration decreases from 5.19 μs to 2.22 μs , which is the typical characteristic of the Q-switched operation. The output power and the single pulse energy of the Q-switched YDFL *versus* pump power are shown in Fig. 6d. One can observe that the output power increases monotonously from 0.52 mW to 2.96 mW and the single pulse energy increases from 24.01 nJ to 81.47 nJ. The increase of pulse repetition frequency with pump

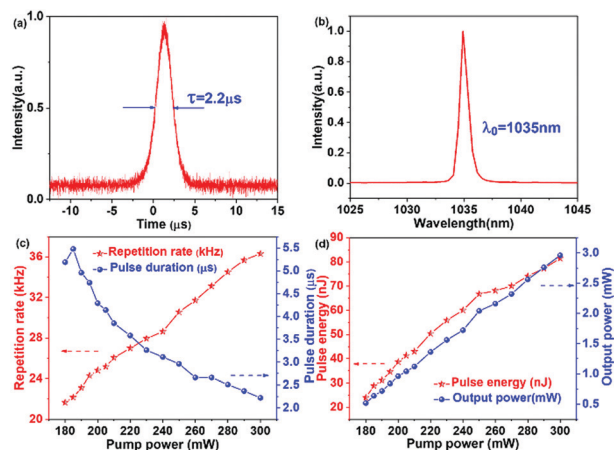


Fig. 6 (a) The Q-switched pulse width at the pump power of 300 mW. (b) The optical spectrum. (c) Pulse repetition rate and pulse duration *versus* pump power. (d) Single pulse energy and average output power vary with pump power.

Table 1 Comparison of this work with other works using different SAs

Year	SA	Repetition rate (kHz)	Min. pulse width (μs)	Max. pulse energy (nJ)	Max. output power (mW)	Modulation depth (%)	Saturation intensity (MW cm^{-2})	Wavelength (nm)	Ref.
2017	BP	26–76	2.0	17.8	1.4	1.94	1.21	1064	33
2017	MoSSe	56.7–71.3	1.2	18.9	1.3	25.0	0.002	1038.5	29
2018	WTe ₂	19.08–79.16	1.0	28.3	2.2	2.18	1.2	1044	34
2018	ReS ₂	52–134	1.56	13.02	3.2	44	8.4	1047	35
2019	ReSe ₂	31.6–68.7	2.87	81.62	5.61	28	9.56	1054.23	36
2019	ReS _{1.02} Se _{0.98}	21.66–31.33	2.22	81.47	2.96	2.9	0.13	1035	This work

power is due to the faster saturation cycle in the laser gain medium and saturable absorber under higher pump power. Similarly, the decrease in pulse width reflects the decrease in time required for each charging and discharging cycle in the laser cavity.³²

Although the output power grows with increasing pump power, the light conversion efficiency is still relatively low. This result may come from the various losses induced by the optical components, splicing losses and jumper losses connected to the SA. We believe that the pulse energy could be further improved by optimizing the cavity design and intracavity parameters. If the pump power was increased further, the Q-switched state will be unstable, which may be attributed to oversaturation rather than thermal damage. The stable Q-switched phenomenon can be observed again by decreasing the pump power. Table 1 shows the comparison between the reported results of this work with previously published results using different SAs with the gain medium of a YDF.

Noise-like pulse generation

Although we obtained a stable Q-Switched pulse train, no mode-locking phenomenon was observed when we increased the pump power and adjusted PC. To adjust dispersion and cavity losses, we reduced the melting fiber point and used 27 cm long YDF and 30% OC to realize mode-locking operation in the fiber cavity, as shown in Fig. 7. In our previous work, we found that the formation of mode-locking operation is related to the polarization state of the laser in the cavity, so we added a PC to regulate it precisely.

In this experiment, the mode-locking can be achieved when the pump power is increased to 270 mW by adjusting the paddles of the PC. The repetition is stable at 34.77 MHz. Self-

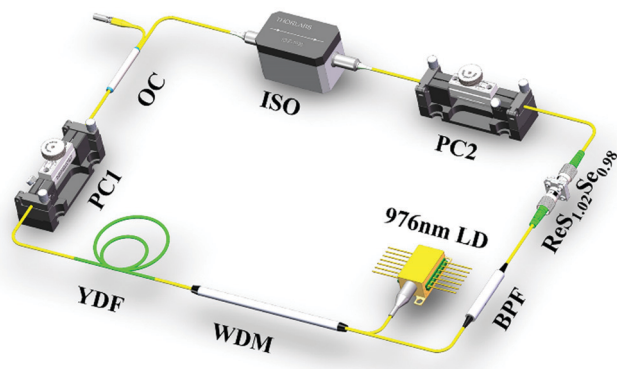


Fig. 7 Diagram of the mode-locked fiber setup.

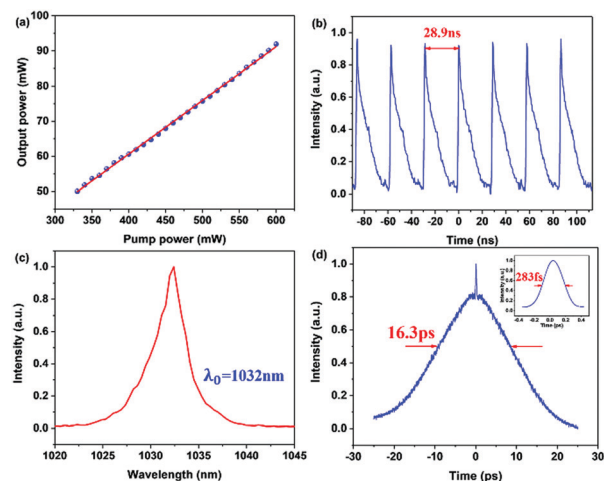


Fig. 8 The NLPs state. (a) Output power of the noise-like pulses versus pumping power. (b) The oscilloscope traces. (c) Optical spectrum. (d) Output pulse train; inset: magnified autocorrelation curve of the NLPs.

start noise-like operation can be maintained over a range of pumping powers (330–600 mW, limited by the pump source). The corresponding output power varies from 50 to 91.9 mW, as shown in Fig. 8a. Fig. 8b shows the oscilloscope trace of the NLPs, indicating that the time interval of the adjacent pulses is 28.9 ns. As presented in Fig. 8c, the measured 3 dB bandwidth of the spectrum (center wavelength 1032 nm) is 3.9 nm at a certain pulse power of 450 mW. The autocorrelation trace clearly shows a narrow coherent spike on a wide base, as shown in Fig. 8d. The full width at half maximum of the noise-like spike is 283 fs in duration. When the pump power is 600 mW, the output power is 91.9 mW, corresponding to a pulse energy of 2.64 nJ. These characteristics are consistent with the typical features of the NLPs.³⁷ Therefore, we can confirm that the soliton state is a typical NLP regime.

Conclusions

In summary, we demonstrated the Q-switched and NLP generation in an all-normal-dispersion Yb-doped fiber laser near 1 μm based on ReS_{1.02}Se_{0.98} SA. In the Q-switched state, with a center wavelength of 1035 nm, the maximum single pulse energy and minimum pulse duration are 81.47 nJ and 2.22 μs respectively. We obtained the fundamental noise-like mode-locked pulses with the center wavelength and 3 dB spectral width measured to be 1032 nm and 3.9 nm, respectively. The maximum output

power was 91.9 mW, corresponding to a single pulse energy of 2.64 nJ. The experimental results show that $\text{ReS}_{1.02}\text{Se}_{0.98}\text{-SA}$ can achieve good performance in noise-like mode-locking fiber lasers.

Conflicts of interest

There are no conflicts to declare.

Acknowledgements

We thank Dr Xin Chen for providing helpful assistance with this work. This work was partly supported by the National Key R&D Program of China (No. 2018YFB1107200), Open Research Fund of State Key Laboratory of Pulsed Laser Technology and the National Science Foundation of China (No. 61675158 and 21673058), the Key Research Program of Frontier Sciences of CAS (QYZDB-SSW-SYS031), and the Strategic Priority Research Program of Chinese Academy of Sciences (XDB30000000).

References

- B. Guo, *Chin. Opt. Lett.*, 2018, **16**, 020004.
- Z. Luo, Y. Huang, M. Zhong, Y. Li, J. Wu, B. Xu, H. Xu, Z. Cai, J. Peng and J. Weng, *J. Lightwave Technol.*, 2014, **32**, 4077–4084.
- M. Skorczakowski, J. Swiderski, W. Pichola, P. Nyga, A. Zajac, M. Maciejewska, L. Galecki, J. Kasprzak, S. Gross, A. Heinrich and T. Bragagna, *Laser Phys. Lett.*, 2010, **7**, 498–504.
- X. L. Qi and S. C. Zhang, *Rev. Mod. Phys.*, 2010, **83**, 175–179.
- Y. Ando, *J. Phys. Soc. Jpn.*, 2013, **82**, 102001.
- Y. Chen, G. Jiang, S. Chen, Z. Guo, X. Yu, C. Zhao, H. Zhang, Q. Bao, S. Wen, D. Tang and D. Fan, *Opt. Express*, 2015, **23**, 12823–12833.
- G. Sobon, *Photonics Res.*, 2015, **3**, A56.
- D. Mao, X. Cui, X. Gan, M. Li, W. Zhang, H. Lu and J. Zhao, *IEEE J. Top. Quantum*, 2018, **24**, 1–6.
- J. Du, M. Zhang, Z. Guo, J. Chen, X. Zhu, G. Hu, P. Peng, Z. Zheng and H. Zhang, *Sci. Rep.*, 2017, **7**, 42357.
- S. Yamashita, Y. Inoue, S. Maruyama, Y. Murakami, H. Yaguchi, M. Jablonski and S. Y. Set, *Opt. Lett.*, 2004, **29**, 1581.
- M. Horowitz, Y. Barad and Y. Silberberg, *Opt. Lett.*, 1997, **22**, 799–801.
- D. Y. Tang, L. M. Zhao and B. Zhao, *Opt. Express*, 2005, **13**, 2289–2294.
- L. M. Zhao, D. Y. Tang and J. Wu, *Opt. Express*, 2007, **15**, 2145–2150.
- Y. Jeong, L. A. Vazquez-Zuniga, S. Lee and Y. Kwon, *Opt. Fiber Technol.*, 2014, **20**, 575–592.
- W. Zhang, Y. Song, H. Guoyu, R. Xu, Z. Dong, K. Li, J. Tian and S. Gong, *Opt. Eng.*, 2017, **56**, 1.
- S. Liu, F. Yan, Y. Li, L. Zhang, Z. Bai, H. Zhou and Y. Hou, *Photonics Res.*, 2016, **4**, 318–321.
- S.-S. Lin, S.-K. Hwang and J.-M. Liu, *Opt. Express*, 2015, **23**, 18256–18268.
- Z. Wang, Z. Wang, Y. Liu, W. Zhao, H. Zhang, S. Wang, G. Yang and R. He, *Opt. Express*, 2016, **24**, 14709.
- G. Sobon, J. Sotor, A. Przewolka, I. Pasternak, W. Strupinski and K. Abramski, *Opt. Express*, 2016, **24**, 20359–20364.
- Y. Chen, M. Wu, P. Tang, S. Chen, J. Du, G. Jiang, Y. Li, C. Zhao, H. Zhang and S. Wen, *Laser Phys. Lett.*, 2014, **11**, 055101.
- J. Liu, S. Zhang, X. Li, M. Han, H. Han, D. Yan, C. Shang and Y. Feng, *High-Power Lasers and Applications VIII. International Society for Optics and Photonics*, 2016.
- Y. Chen, S. Chen, J. Liu, Y. Gao and W. Zhang, *Opt. Express*, 2016, **24**, 13316.
- Z. Wang, Z. Wang, Y. Liu, R. He, S. Han, G. Wang, G. Yang and X. Wang, *Laser Phys. Lett.*, 2018, **15**, 085103.
- E. J. Aiub, D. Steinberg, E. A. Thoroh de Souza and L. A. M. Saito, *Opt. Express*, 2017, **25**, 10546.
- W. Liu, L. Pang, H. Han, M. Liu, M. Lei, S. Fang, H. Teng and Z. Wei, *Opt. Express*, 2017, **25**, 2950–2959.
- D. Mao, X. She, B. Du, D. Yang, W. Zhang, K. Song, X. Cui, B. Jiang, T. Peng and J. Zhao, *Sci. Rep.*, 2016, **6**, 23583.
- K. F. Mak, C. Lee, J. Hone, J. Shan and T. F. Heinz, *Phys. Rev. Lett.*, 2010, **105**, 136805.
- K. Wang, J. Wang, J. Fan, M. Lotya, A. Gallagher, D. S. Fox, Y. Feng, X. Zhang, B. X. Jiang, Q. Zhao, H. Zhang, J. Coleman, L. Zhang, W. J. Blau and C. Name, *ACS Nano*, 2013, **7**, 9260–9267.
- H. Ahmad, S. A. Reduan, S. N. Aidit and Z. C. Tiu, *Chin. Opt. Lett.*, 2017, **15**, 020601.
- W. Wen, Y. Zhu, X. Liu, H.-P. Hsu, Z. Fei, Y. Chen, X. Wang, M. Zhang, K.-H. Lin, F.-S. Huang, Y.-P. Wang, Y.-S. Huang, C.-H. Ho, P.-H. Tan, C. Jin and L. Xie, *Small*, 2017, **13**, 1603788.
- C. H. Ho, Y. S. Huang, P. C. Liao and K. K. Tiong, *J. Phys. Chem. Solids*, 1999, **60**, 1797–1804.
- H. Ahmad, S. I. Ooi, Z. C. Tiu and B. M. A. Rahman, *Opt. Commun.*, 2018, **426**, 1–8.
- K.-X. Huang, B.-L. Lu, D. Li, X.-Y. Qi, H.-W. Chen, N. Wang, Z.-R. Wen and J.-T. Bai, *Appl. Opt.*, 2017, **56**, 6427.
- S. Ko, J. Lee and J. H. Lee, *Chin. Opt. Lett.*, 2018, **16**, 020017.
- B. L. Lu, K. X. Huang, X. Y. Qi, Z. R. Wen, N. Wang, H. W. Chen and J. T. Bai, *IEEE J. Sel. Top. Quantum Electron.*, 2018, DOI: 10.1109/JSTQE.2018.2885493.
- N. Wang, B. L. Lu, X. Y. Qi, Y. Jiao, Z. R. Wen, H. W. Chen and J. T. Bai, *Opt. Laser Technol.*, 2019, **116**, 300–304.
- L. M. Zhao, D. Y. Tang and J. Wu, *Opt. Express*, 2007, **15**, 2145–2150.